

1 Thyrotropin-releasing-hormone-synthesizing neurons of the hypothalamic paraventricular  
2 nucleus are inhibited by glycinergic inputs

3

4 Edina Varga<sup>1\*</sup>, Erzsébet Farkas<sup>1\*</sup>, Györgyi Zséli<sup>1</sup>, Andrea Kádár<sup>1</sup>, Alexandra Venczel<sup>1</sup>, Dóra  
5 Kóvári<sup>1</sup>, Dorottya Németh<sup>1</sup>, Zoltán Máté<sup>2</sup>, Ferenc Erdélyi<sup>2</sup>, András Horváth<sup>3,4</sup>, Ottó Szenci<sup>3,4</sup>,  
6 Masahiko Watanabe<sup>5</sup>, Ronald M. Lechan<sup>6,7</sup>, Balázs Gereben<sup>1</sup> and Csaba Fekete<sup>1,6</sup>

7

8 <sup>1</sup>Department of Endocrine Neurobiology, Institute of Experimental Medicine, Hungarian  
9 Academy of Sciences, Budapest, Hungary H-1083

10 <sup>2</sup>Medical Gene Technology Unit, Institute of Experimental Medicine, Hungarian  
11 Academy of Sciences, Budapest, Hungary H-1083

12 <sup>3</sup>Department and Clinic for Production Animals, University of Veterinary Medicine Budapest,  
13 Üllő, Dóra Major, Hungary, H-2225

14 <sup>4</sup>MTA–SZIE Large Animal Clinical Research Group, Üllő, Dóra major, Hungary, H-2225

15 <sup>5</sup>Department of Anatomy, Hokkaido University School of Medicine, Sapporo 060-8638,  
16 Japan

17 <sup>6</sup>Department of Medicine, Division of Endocrinology, Diabetes and Metabolism, Tupper  
18 Research Institute, Tufts Medical Center, Boston, MA, USA 02111.

19 <sup>7</sup>Department of Neuroscience, Tufts University School of Medicine, Boston, MA, USA 02111.

20 \*Contributed equally to the work

21

22 Running title: Glycinergic innervation of TRH neurons in the PVN

23 Keywords: Hypophysiotropic TRH neurons, hypothalamic paraventricular nucleus,  
24 innervation, glycine, patch-clamp electrophysiology

25

26 Corresponding author: Csaba Fekete MD PhD [fekete.csaba@koki.mta.hu](mailto:fekete.csaba@koki.mta.hu)

27

28

29 **Abstract**

30 **Background:** Glycine is a classical neurotransmitter that has role in both inhibitory and  
31 excitatory synapses. To understand whether glycinergic inputs are involved in the regulation of  
32 the hypophysiotropic thyrotropin-releasing hormone (TRH) neurons, the central controllers of  
33 the hypothalamic-pituitary-thyroid (HPT) axis, the glycinergic innervation of the TRH neurons  
34 was studied in the hypothalamic paraventricular nucleus (PVN).

35 **Methods:** Double-labeling immunocytochemistry and patch clamp electrophysiology was used  
36 to determine the role of the glycinergic neurons in the regulation of TRH neurons in the PVN.  
37 Anterograde- and retrograde tracing methods were used to determine the sources of the  
38 glycinergic input of TRH neurons.

39 **Results:** Glycine transporter 2 (GLYT2), a marker of glycinergic neurons, containing axons  
40 was found to establish symmetric type of synapses on TRH neurons in the PVN. Furthermore,  
41 glycine receptor-immunoreactivity was observed in these TRH neurons. The raphe magnus  
42 (RMg) and the ventrolateral periaqueductal gray (VLPAG) were found to be the exclusive  
43 sources of the glycinergic innervation of the TRH neurons within the PVN.

44 Patch-clamp electrophysiology using sections of TRH-IRES-tdTomato mice showed that  
45 glycine hyperpolarized the TRH neurons and completely blocked the firing of these neurons.  
46 Glycine also markedly hyperpolarized the TRH neurons in the presence of tetrodotoxin  
47 demonstrating the direct effect of glycine. In more than 60% of the TRH neurons, spontaneous  
48 inhibitory postsynaptic currents (sIPSC) were observed, even after the pharmacological  
49 inhibition of glutamatergic and GABAergic neuronal transmission. The glycine antagonist,  
50 strychnine, almost completely abolished these sIPSCs, demonstrating the inhibitory nature of  
51 the glycinergic input of TRH neurons.

52 **Conclusions:** These data demonstrate that TRH neurons in the PVN receive glycinergic inputs  
53 from the RMg and the VLPAG. The symmetric type of synaptic connection and the results of  
54 the electrophysiological experiments demonstrate the inhibitory nature of these inputs.

55

56 **INTRODUCTION**

57 Glycine is a classical neurotransmitter that has an important role in both inhibitory and  
58 excitatory synapses (1). Glycinergic neurons are primarily located in the brainstem and spinal  
59 cord (2), however, glycinergic axons are also observed in the hypothalamus (3). Two glycine-  
60 transporter subtypes (GlyT) were identified in the central nervous system: glycine transporter-  
61 1 (GlyT1), mainly located in glial cells and nerve terminals of excitatory neurons, and glycine  
62 transporter-2 (GlyT2), present exclusively in glycinergic neurons (4, 5).

63 Glycine is released from inhibitory, presynaptic terminals and binds to strychnine-sensitive  
64 glycine receptors that are located in the postsynaptic membrane of target cells (1). Activation  
65 of glycine receptors leads to influx of chloride ions into the cytoplasm and thereby, inhibits the  
66 postsynaptic neuron (6). In addition, glycine is also important for excitatory glutamatergic  
67 neurotransmission because it serves as an essential co-agonist of glutamate at NMDA receptors  
68 (7).

69 The hypothalamic paraventricular nucleus (PVN), where hypophysiotropic thyrotropin-  
70 releasing hormone- (TRH)-synthesizing neurons, the main central regulators of the  
71 hypothalamic-pituitary-thyroid (HPT) axis reside(8), is densely innervated by glycinergic  
72 axons (3). Within the PVN, glycine has been shown to elicit large, inward currents (9).  
73 Furthermore, evoked glycinergic currents can be observed in parvocellular PVN neurons in the  
74 presence of the blockers of glutamate and GABA receptors (9), suggesting that ascending  
75 glycinergic pathways regulate parvocellular neurons in the PVN.

76 Based on these data, we hypothesized that glycinergic brainstem neurons are involved in the  
77 regulation of the TRH neurons in the PVN including the hypophysiotropic TRH neurons. To  
78 test this hypothesis, we performed neuroanatomical and electrophysiological experiments.  
79 Since TRH neurons are dispersed in the PVN, identification of these cells was difficult in  
80 electrophysiological studies. In addition, in morphological studies, the cell bodies of TRH

81 neurons could only be identified after inhibition of axonal transport by colchicine treatment.  
82 Therefore, to facilitate both the electrophysiological and morphological studies, we generated  
83 a TRH-IRES-tdTomato knock in mouse line in which the TRH neurons can be easily identified  
84 based on the presence of the red fluorescent protein in their perikarya.

85 **Materials and methods**

86 *Animals*

87 The experiments were carried out in adult, male, CD1 mice (N=8), GlyT2::GFP mice (N=9)  
88 (3), TRH-IRES-tdTomato mice (N=30), double transgenic mice heterozygous for TRH-IRES-  
89 tdTomato and GlyT2::Cre (10) (TRH-IRES-tdTomato//GlyT2::Cre; N=10), and, weighing 30–  
90 40 g, housed under standard environmental conditions (light between 06:00 and 18:00 h,  
91 temperature  $22\pm 1^{\circ}\text{C}$ , rat chow and water *ad libitum*). The *in vitro* patch clamp  
92 electrophysiology studies were performed on mice between P40 and P60 days of age. All  
93 experimental protocols were reviewed and approved by the Animal Welfare Committee at the  
94 Institute of Experimental Medicine of the Hungarian Academy of Sciences.

95

96 *Generation of the TRH-IRES-tdTomato mouse line*

97 An IRES tdTomato cassette was inserted into the mouse TRH locus using CRISPR/Cas9 (11)  
98 on FVB.129P2-Pde6b<sup>+</sup> Tyr<sup>c-ch</sup>/AntJ (FVB/Ant) background. The 1473 bp long 5' and the  
99 1375bp long 3' TRH arms were obtained by PCR on FVB/Ant gDNA (5' TRH arm sense  
100 oligonucleotide: ccgctcgagCACCTTGGCACCCTGATACCAGGAA; antisense:  
101 tccccgcggTTACTCCTCC AGAGGTTCCCTGA; 3' TRH arm sense:  
102 ataagaatcggccgctGGTTAGAGTCAGGCTTT AGGTCTA; antisense: ctagctagc  
103 CTGGCATGGTGACTCATCTATAACAT). The 5' arm was cloned between XhoI and SacII  
104 followed by IRES of the pPRIG vector (12) between SacII and EcoRI and the tdTomato coding  
105 region between EcoRI and NotI sites. The 3' arm was placed between NotI and NheI. The  
106 construct was assembled in a D10 vector and confirmed by sequencing.

107 Pronuclear microinjection was carried out on fertilized eggs of FVB/Ant mice, using of a single  
108 guide RNA with the target sequence of GGAGTAAGGTTAGAGTC and Cas9 mRNA  
109 (Trilink).

110 Founders were identified with qPCR for tdTomato (tdTomF GCTCCAAGGCGTACGTGAA,  
111 tdTomR GGAAGGACAGCTTCTTGTAATCG, tdTom\_probe 6-FAM-  
112 CACCCCGCCGACAT-MGBNFQ) followed by checking the insertion sites with outer and  
113 inner PCR oligos (CTTCCATGAGAGGAGTATTTATCA,  
114 CATGGACGAGCTGTACAAGTA, GGCCGCTATGACTTTAGCTTC,  
115 CTTACACCCACTGCCTTTGAC and GTAGTCAGGCACGTCGTATGG). A founder with a  
116 single copy of the targeting cassette was selected for breeding.

117 Heterozygote F1 animals were crossbred with littermate animals of identical genotype. Mice  
118 were bred and maintained as homozygous colonies.

119

#### 120 *Characterization of the TRH-IRES-tdTomato mice*

121 All solutions were made with MilliQ water treated with diethylpyrocarbonate (DEPC, 0.2µl/ml)  
122 overnight and then autoclaved. TRH-IRES-tdTOMATO mice (N=6) were deeply anesthetized  
123 with ketamine/xylazine (ketamine 50 mg/kg, xylazine 10 mg/kg body weight, ip) and the  
124 animals perfused transcardially with 10 ml 0.01 M PBS, pH 7.4, followed by 50 ml of 4% PFA  
125 in 0.1 M PB, pH 7.4. The brains were quickly removed, postfixed by immersion in the same  
126 fixative for 2 hours at RT, cryoprotected in 20% sucrose in PBS at 4°C overnight and then  
127 frozen using powdered dry ice. Serial 20-µm-thick coronal sections through the whole brain  
128 were cut on a cryostat (Leica Microsystems, Wetzlar, Germany), collected in freezing solution  
129 and stored at -20°C until used.

130 The digoxigenin-labeled antisense mouse pro-TRH cRNA probe was synthesized using a 741-  
131 base (corresponding to the 106–846 nucleotides of the mouse TRH mRNA; BC053493) cDNA  
132 template (13) as described earlier (14). The hybridization was performed in 200 µl  
133 polypropylene tubes in a hybridization buffer (50% formamide, 2× SSC, 10% dextran sulfate,  
134 0.5% SDS, 250 µg/ml denatured salmon sperm DNA) containing the digoxigenin-labeled probe

135 (1:100 dilution) for 16 hr at 56°C. The sections were washed in 1× SSC for 15 min and then  
136 treated with RNase (25 µg/ml) for 1 hr at 37°C. After additional washes in 0.1× SSC (four times  
137 for 15 min each) at 65°C, sections were washed in PBS, treated with the mixture of 0.5% Triton  
138 X-100 and 0.5% H<sub>2</sub>O<sub>2</sub> for 15 min, and then with 2% BSA in PBS for 20 min to reduce the  
139 nonspecific antibody binding. The sections were incubated with a mixture of sheep anti-  
140 digoxigenin-peroxidase Fab fragments (1:100; Boehringer Mannheim) and rabbit anti-RFP  
141 serum (Rockland Immunochemicals Inc., Limerick, PA, USA, Indianapolis, IN, USA) diluted  
142 at 1:3000 in 1% BSA in PBS for 2 d at 4°C. The sections were rinsed in PBS and then the in  
143 situ hybridization signal was amplified using the TSA amplification kit according to the  
144 manufacturer's instructions. After further washes, the sections were incubated in a mixture of  
145 Fluorescein DTAF-conjugated Streptavidin (1:300, Jackson ImmunoResearch Labs, West  
146 Grove, PA, USA) and Alexa 555-conjugated donkey anti-rabbit IgG (1:500, Jackson  
147 ImmunoResearch Labs, West Grove, PA) for 2 hours and mounted glass slides. Slides were air  
148 dried and coverslipped with Vectashield mounting medium (Vector Laboratories Inc,  
149 Burlingame, CA, USA). Images were taken with a Zeiss LSM 780 laser scanning confocal  
150 microscope.

151

#### 152 *Generation of a sheep antibody against tdTomato*

153 The tdTomato coding region was inserted into a pET26b (+) vector (Merck, Darmstadt,  
154 Germany) by adding a C-terminal His-tag. Recombinant expression of His-tagged tdTomato  
155 was performed in Rosetta 2(DE3) E. Coli strain (Merck, Darmstadt, Germany). Induction was  
156 performed at 18 °C with 0.5 mM IPTG and the recombinant protein was expressed overnight.  
157 The cells were harvested by centrifugation at 4000xg for 30 min at 4 °C and the pellet was  
158 stored at -20 °C then resuspended in 20 ml lysis buffer (50 mM Tris base, 0.2 M NaCl, 5 %  
159 glycerin, 1 mM DTT, 1 mM TCEP, 1 mM PMSF supplemented with Roche Complete, Mini,



160 EDTA-free Protease Inhibitor Cocktail, pH 7.5) followed by lysis with 500 µg/ml lysozyme at  
161 4 °C for 4 h and further incubation with 5 mM MgCl<sub>2</sub> and 1 mg/ml DNase. The His-tagged  
162 tdTomato was purified on 3 ml Ni-NTA column (ThermoFisher, Waltham, MA, USA)  
163 equilibrated with column buffer (20 mM Tris base, 200 mM NaCl, pH 7.5). After washing the  
164 column with 75 mM imidazole containing column buffer pure tdTomato fraction was eluted  
165 with 500 mM imidazole column buffer at pH 7.5. The eluted fraction was analyzed by SDS-  
166 PAGE and dialyzed against 0.1M PBS.

167 760 µg tdTomato in 1 ml PBS was emulsified with an equal volume of Freund's complete  
168 adjuvant (Sigma-Aldrich, St. Louis, MO, USA) and injected subcutaneously into sheep.  
169 Subsequent boosts with Freund's incomplete adjuvant were administered at 28-day intervals.  
170 Eight days after the fourth immunization, blood was collected and the serum was separated by  
171 centrifugation.

172

### 173 *Animal preparation for examination of the glycinergic input to TRH neurons in the PVN*

174 CD1 mice (N=8) were deeply anesthetized with ketamine/xylazine (ketamine 50 mg/kg,  
175 xylazine 10 mg/kg body weight, intraperitoneal (ip)) and the animals perfused transcardially  
176 with 10 ml 0.01 M phosphate-buffered saline (PBS), pH 7.4, followed sequentially by 50 ml of  
177 2% paraformaldehyde (PFA) / 4% acrolein in 0.1 M phosphate buffer (PB), pH 7.4, and then  
178 by 20 ml of 2% PFA in the same buffer. The brains were rapidly removed and stored in 4%  
179 PFA for 2 h for light microscopy (N=4) at room temperature (RT), or 24 h for electron  
180 microscopy (N=4) at 4°C.

181

### 182 *Sectioning and section pretreatment for light microscopic studies*

183 The brains were cryoprotected in 30% sucrose in PBS at 4°C overnight, then frozen using  
184 powdered dry ice. Serial, 25 µm thick coronal sections through the PVN were cut on a freezing

185 microtome (Leica Microsystems, Wetzlar, Germany), collected in cryoprotectant solution (30%  
186 ethylene glycol; 25% glycerol; 0.05 M PB) and stored at -20°C until used. Series of sections  
187 from each brain were treated with 1% sodium borohydride (Sigma-Aldrich, St. Louis, MO,  
188 USA) in distilled water (DW) for 30 min and with a mixture of 0.5% Triton X-100 and 0.5%  
189 H<sub>2</sub>O<sub>2</sub> in PBS for 15 min. To reduce nonspecific antibody binding, the sections were treated with  
190 2% normal horse serum (NHS) in PBS for 20 min.

191

192 *Double-labeling immunofluorescence for examination of the glycinergic input of TRH neurons*  
193 *in the PVN*

194 Pretreated sections of CD1 mice were incubated in a mixture of rabbit anti-GlyT2 IgG (15, 16)  
195 and sheep anti-TRH IgG (1:4000) (17) in PBS containing 2% NHS and 0.2% sodium-azide  
196 (antiserum diluent) for 2 days at 4°C. After rinses in PBS, the sections were incubated in a  
197 mixture of Alexa 555-conjugated donkey anti-rabbit IgG (1:500, Jackson ImmunoResearch Labs,  
198 West Grove, PA, USA) and Alexa 488-conjugated donkey anti-sheep IgG (1:500, Jackson  
199 ImmunoResearch Labs, West Grove, PA, USA) in antiserum diluent. After rinses in PBS, the  
200 sections were mounted onto glass slides, and coverslipped with Vectashield mounting medium  
201 (Vector Laboratories Inc, Burlingame, CA, USA).

202

203 *Double labeling immuno- electron microscopy for examination of the glycinergic input of TRH*  
204 *neurons in the PVN*

205 Serial, 25µm thick coronal sections were cut on a Leica VT 1000S vibratome (Leica  
206 Microsystems, Wetzlar, Germany) through the rostro-caudal extent of the PVN and collected  
207 in PBS. The sections were treated with 1% sodium borohydride (Sigma-Aldrich, St. Louis, MO,  
208 USA) in 0.1 M PB for 30 min, followed by 0.5% H<sub>2</sub>O<sub>2</sub> in PBS for 15 min. The sections were  
209 cryoprotected in 15% sucrose in PBS for 15 min at RT and in 30% sucrose in PBS overnight at

210 4°C and then, quickly frozen over liquid nitrogen and thawed at RT. This freezing-thawing  
211 cycle was repeated 3 times to improve antibody penetration. To reduce the nonspecific antibody  
212 binding, the sections were treated with 2% NHS in PBS for 20 min. Sections were placed into  
213 a mixture of rabbit anti-GlyT2 IgG (1µg/ml) and sheep anti-TRH IgG (1:1000) for 4 days at  
214 4°C. After rinsing in PBS and in a mixture of 0.1% cold water fish gelatin (Aurion, Wageningen,  
215 Netherlands) and 1% BSA (Sigma-Aldrich, St. Louis, MO, USA) in PBS, the sections were  
216 incubated in a cocktail of donkey anti-sheep IgG-conjugated with 0.8 nm colloidal gold (1:100,  
217 Electron Microscopy Sciences, Fort Washington, PA, USA) and biotinylated donkey anti-rabbit  
218 IgG (1:500, Jackson Immunoresearch Labs, West Grove, PA, USA) in the same cold water fish  
219 gelatin- and BSA-containing solution for 20 h at 4°C. After washing in PBS, the sections were  
220 fixed in 1.25% glutaraldehyde (Electron Microscopy Sciences, Fort Washington, PA, USA) in  
221 0.1M PB for 10 min. The gold particles were silver intensified with the Aurion R-Gent SE-LM  
222 Kit (Aurion, Wageningen, Netherlands) (18). After rinsing in 0.2M sodium citrate, pH 7.5, the  
223 sections were immersed in ABC Elite Complex (1:1000, Vector Laboratories Inc, Burlingame,  
224 CA, USA) diluted in 0.05M TRIS buffer for 1 hour at RT. The GlyT2 immunoreactivity was  
225 detected with NiDAB developer (0.025% DAB/0.0036% H<sub>2</sub>O<sub>2</sub> in 0.05 M Tris buffer, pH 7.6).  
226 The sections were osmicated, and then treated with 2% uranyl acetate in 70% ethanol for 30  
227 min. Following dehydration in an ascending series of ethanol and acetonitrile, the sections were  
228 flat embedded in Durcupan ACM epoxy resin (Fluka, Sigma-Aldrich, St. Louis, MO, USA) on  
229 liquid release agent (Electron Microscopy Sciences, Fort Washington, PA, USA)-coated slides,  
230 and polymerized at 56 °C for 2 days. Ultrathin 50–60 nm sections were cut with Leica ultracut  
231 UCT ultramicrotome (Leica Microsystems, Wetzlar, Germany), collected onto Formvar-  
232 coated, single slot grids, and examined with a JEOL electron microscope (Jeol, Tokyo, Japan).  
233

234 *Tissue preparation for the examination of the glycine receptor (GlyR) content of TRH neurons*  
235 *in the PVN*

236 TRH-IRES-tdTomato mice (N=5) were deeply anesthetized with ketamine/xylazine (ketamine  
237 50 mg/kg, xylazine 10 mg/kg body weight, ip) and perfused transcardially with 10 ml 0.01 M  
238 PBS, pH 7.4, followed by 50 ml of 4% PFA in 0.1 M PB, pH 7.4. The brains were rapidly  
239 removed, postfixed in 4% PFA for 2 hours at RT and cryoprotected in 30% sucrose in 0.01 M  
240 PBS overnight at room temperature. The brains were then frozen with powdered dry ice and  
241 stored at -20°C until use.

242 Serial, 25 µm thick coronal sections through the PVN were cut on a freezing microtome,  
243 collected in cryoprotectant solution and stored at -20°C until use.

244 Series of sections from each brain were subjected to pepsin pretreatment to facilitate antigen  
245 exposure (16). The sections were incubated in 1 mg/ml pepsin (Dako Agilent, Santa Clara, CA,  
246 USA) for 7 min at 37 °C. After washing in PBS, the sections were treated with 0.5% Triton X-  
247 100/0.5% H<sub>2</sub>O<sub>2</sub> in PBS for 15 min, immersed in 2% NHS in PBS for 20 min and then incubated  
248 in a mixture of guinea pig-GlyRa IgG (15) (16) and rabbit-RFP antiserum (1:3000, Rockland  
249 Immunochemicals Inc., Limerick, PA, USA) in antiserum diluent for 2 days at 4°C. After rinses  
250 in PBS, the sections were incubated in biotinylated donkey anti-guinea pig IgG (1:500, Jackson  
251 Immunoresearch Labs, West Grove, PA, USA) for two hours and in ABC Elite Complex  
252 (1:1000, Vector Laboratories Inc, Burlingame, CA, USA) in 0.05M TRIS buffer for an hour.  
253 The immunoreaction was amplified with biotinylated tyramide using the TSA amplification kit  
254 (Perkin Elmer Life and Analytical Sciences, Waltham, MA, USA). After further washes, the  
255 sections were incubated in a mixture of the Fluorescein DTAF-conjugated Streptavidin (1:300,  
256 Jackson Immunoresearch Labs, West Grove, PA, USA) and Alexa 555-conjugated donkey anti-  
257 rabbit IgG (1:500, Jackson Immunoresearch Labs, West Grove, PA, USA), mounted onto glass

258 slides and coverslipped with Vectashield mounting medium (Vector Laboratories Inc,  
259 Burlingame, CA, USA).

260

261 *Retrograde tract-tracing and tissue preparation for the identification of the sources of the*  
262 *glycinergic innervation of the PVN*

263 The retrograde tracer, cholera toxin  $\beta$  subunit (CTB; List Biological Labs, Campbell, CA,  
264 USA), was injected by iontophoresis into the PVN of GlyT2/GFP mice (N=9). The animals  
265 were anesthetized ip with ketamine-xylazine (ketamine: 50 mg/kg; xylazine: 10 mg/kg body  
266 weight) and their head positioned in a stereotaxic apparatus with the Bregma and Lambda in  
267 the horizontal plane. Through a burr hole in the skull, a glass micropipette (17.5-20  $\mu$ m outer  
268 tip diameter) filled with 0.5% CTB in 0.01M PB at pH 8.0 was lowered into the brain at  
269 stereotaxic coordinates corresponding to the PVN (anterior–posterior, -0.9 mm from the  
270 Bregma; lateral, -0.15 mm; and dorsoventral, -4.8 mm from the surface of the skull), based on  
271 the atlas of Paxinos and Watson (19). CTB was deposited over 3 min of positive current (4  $\mu$ A,  
272 pulsed on—off at 7s intervals) using a constant-current source (Stoelting, Wood Dale, IL,  
273 USA). The animals were anesthetized 7–10 days after tracer deposition and perfused with 10  
274 ml PBS, pH 7.4, followed by 50 ml of 4% paraformaldehyde in 0.1 M PB, pH 7.4. The brains  
275 were rapidly removed, postfixed in 4% PFA for 2 hours at RT, cryoprotected in 30% sucrose  
276 in PBS overnight at RT, then frozen using powdered dry ice and stored at -20°C until use.  
277 Twenty-five- $\mu$ m-thick coronal sections were cut on a freezing microtome into one-in-four  
278 series of sections.

279

280 *Immunohistochemically identification of the CTB injection sites*

281 Series of sections was pre-treated as described above and then incubated in goat anti-CTB  
282 serum (1:10000, List Biological Labs, Campbell, CA, USA) for 2 days. Following washes in

283 PBS, the sections were immersed in biotinylated donkey anti-sheep IgG (1:500, Jackson  
284 Immunoresearch Labs, West Grove, PA, USA) for 2 h and in ABC (1:1000, ABC Elite, Vector  
285 Laboratories Inc, Burlingame, CA, USA) diluted in 0.05M Tris buffer for one hour. Following  
286 rinses in PBS, peroxidase activity was visualized with NiDAB developer. The sections were  
287 mounted on gelatin coated slides, air dried, counterstained with 1% cresyl-violet and  
288 coverslipped with DPX mounting medium (Sigma-Aldrich, St. Louis, MO, USA).

289

290 *Double-labeling immunofluorescence for the identification of the sources of the glycinergic*  
291 *input of the PVN*

292 One of the four series of sections was pre-treated as described above and incubated in a mixture  
293 of goat anti-CTB serum (1:5000, List Biological Labs, Campbell, CA, USA) and rabbit anti-  
294 GFP serum (1:0,000, Life technologies) for 2 days at 4°C. Then, the sections were immersed in  
295 biotinylated donkey anti-sheep IgG (1:500, Jackson Immunoresearch Labs, West Grove, PA,  
296 USA) for 2 h, followed by ABC (1:1000, ABC Elite, Vector Laboratories Inc, Burlingame, CA,  
297 USA) for 2 hours. The immunoreaction product was amplified with TSA amplification kit for  
298 10 min. The signals were visualized by incubation in a mixture of Alexa 488-conjugated donkey  
299 anti-rabbit IgG (1:500, Jackson Immunoresearch Labs, West Grove, PA, USA) and Alexa 555-  
300 conjugated Streptavidin (1:500, Jackson Immunoresearch Labs, West Grove, PA, USA) for two  
301 hours, mounted onto glass slides and coverslipped with Vectashield mounting medium (Vector  
302 Laboratories Inc, Burlingame, CA, USA).

303

304 *Virus injection and tissue preparation for the identification of the sources of the glycinergic*  
305 *innervation of the TRH neurons in the PVN*

306 As our retrograde tract-tracing experiment showed that the VLPAG and the RMg are the  
307 sources of the glycinergic input of the PVN, *DIO-hChr2(H134R)-eYFP adeno-associated virus*

308 (AAV) was injected to the VLPAG (N=5) or RMg (N=5) in *TRH-IRES-tdTomato//GlyT2-Cre*  
309 mice. The Cre expression in the GLYT2 cells allowed the glycinergic neuron specific  
310 expression of the hChR2(H134R)-eYFP fusion protein, while the tdTomato expression of TRH  
311 neurons facilitated the detection of TRH neurons. The surgeries were performed in a BSL-2  
312 AAV facility. The mice were anesthetized ip with ketamine-xylazine (ketamine: 50 mg/kg;  
313 xylazine: 10 mg/kg body weight) and their head positioned in a stereotaxic apparatus with the  
314 Bregma and Lambda in the horizontal plane. Through a burr hole in the skull, a glass pipette  
315 (25- $\mu$ m tip) connected to a Nanoject II/Nanoliter 2000 microinjector (WPI Inc., Sarasota, FL,  
316 USA) was lowered into the brain at stereotaxic coordinates corresponding to the VLPAG  
317 (anteroposterior: -4.72 mm, mediolateral: -0.4 mm, dorsoventral: -2.75 mm), or RMg  
318 (anteroposterior: -5.34 mm, mediolateral: 0 mm, dorsoventral: -5.7mm) based on the atlas of  
319 Paxinos and Watson (19). 80 nl (RMg) and 150 nl (VLPAG) of virus-containing solution (4.5  
320  $\times 10^{12}$  virus/ml, titer:  $1 \times 10^{13}$  GC/ml) was injected unilaterally into the nuclei at a rate of  
321 5nl/sec. Five minutes after the injection, the pipette was slowly removed, the scalp sutured and  
322 the mice housed in BSL-2 quarantine for 2 weeks before experimentation. The animals were  
323 re-anaesthetized and perfused transcardially with 10 ml 0.01 M PBS, pH 7.4, followed by 50  
324 ml of 4% PFA in 0.1 M PB, pH 7.4. The brains were rapidly removed and postfixed in 4% PFA  
325 for 2 hour at RT. The brains were cryoprotected in 30% sucrose in 0.01 M PBS overnight at  
326 room temperature, frozen using powdered dry ice and stored at -20°C until use. Twenty-five-  
327  $\mu$ m-thick coronal sections were cut on a freezing microtome through the PVN and VLPAG or  
328 RMg into one-in-four series of sections.

329

330 *Localization of virus injection sites*

331 Series of sections containing the VLPAG or RMg were mounted onto glass slides and  
332 coverslipped with DAPI containing Vectashield mounting medium (Vector Laboratories Inc,  
333 Burlingame, CA, USA). The injection sites were detected based on the fluorescence of YFP.

334

335 *Tissue preparation for examination of the innervation of TRH neurons by glycinergic neurons*  
336 *of the VLPAG and RMg*

337 Sections of the PVN pre-treated as described above were incubated in a mixture of primary  
338 antisera: rabbit anti-GFP (1:10,000, ThermoFisher, Waltham, MA, USA) and sheep anti-  
339 tdTomato (1:80,000, generated in our laboratory) for 48h. After washing in PBS, sections were  
340 incubated in the cocktail of Alexa 488-conjugated donkey anti-rabbit IgG (1:250, Invitrogen)  
341 and Alexa 555-conjugated donkey anti-sheep IgG (1:500, Invitrogen, Carlsbad, CA, USA) for  
342 2 h, mounted onto glass slides and coverslipped with Vectashield mounting medium.

343

344 *Image analyzes of light microscopic preparations*

345 Images of fluorescent preparations were taken using Zeiss LSM 780 confocal microscope  
346 (Zeiss Company, Jena, Germany) using line by line sequential scanning with laser excitation  
347 lines 490-553 nm for Alexa Fluor 488 and 566-697 nm for Alexa Fluor 555;  
348 beamsplitter/emission filters, MSB488/561 nm for Alexa Fluor 488 and Alexa Fluor 555. For  
349 20x and 63x oil lenses, pinhole sizes were set to obtain optical slices of 2 and 0.7  $\mu\text{m}$  thickness,  
350 respectively, and the series of optical sections were recorded with 0.6  $\mu\text{m}$  Z steps.

351 Images were analyzed with Zen 2012 (Zeiss Company, Jena, Germany) and with Adobe  
352 Photoshop (Adobe System Inc., CA, USA).



353 Images of NiDAB stained preparations were captured with a Zeiss AxioImager M1  
354 microscope using AxioCam MRc 5 digital camera (Zeiss Company, Jena, Germany) and  
355 AxioVision 4.6 software (Zeiss Company, Jena, Germany).

356

#### 357 *Specificity of the used antibodies*

358 The specificity of rabbit anti-GlyT2 IgG (16), sheep anti-TRH IgG (17), guinea pig-GlyRa  
359 IgG (16) was previously described. The rabbit anti-RFP antibody (Rockland Immunochemicals,  
360 Limerick, PA, USA) and the rabbit anti-GFP serum (ThermoFisher, Waltham, MA, USA) did  
361 not generate any immunoreactivity on sections of wild type mice. The goat anti-CTB serum (List  
362 Biological Labs, Campbell, CA, USA) did not give any staining on sections of mice without  
363 tracer injection. The sheep antibody against tdTomato that was generated in our laboratory did  
364 not generate any staining on sections of wild type mice and the antibody did not crossreact with  
365 YFP.

366

#### 367 In vitro Patch-Clamp Electrophysiology

##### 368 *Slice preparation for electrophysiological recordings*

369 TRH-IRES-tdTomato mice (N=9) were deeply anaesthetized with isoflurane and decapitated.  
370 The brains were rapidly removed and immersed in ice-cold slicing solution (in mM: 87 NaCl,  
371 2.5 KCl, 0.5 CaCl<sub>2</sub>, 7 MgCl<sub>2</sub>, 25 NaHCO<sub>3</sub>, 25 D-glucose, 1.25 NaH<sub>2</sub>PO<sub>4</sub>, 75 sucrose) saturated  
372 with 95% O<sub>2</sub>/5% CO<sub>2</sub>. Coronal 250 μm slices were cut using a VT1200S vibratome (Leica  
373 Microsystems, Wetzlar, Germany), then the slices transferred into a holding chamber filled with  
374 artificial cerebrospinal fluid (aCSF; 36°C; in mM: 126 NaCl, 2.5 KCl, 26 NaHCO<sub>3</sub>, 2 CaCl<sub>2</sub>, 2  
375 MgCl<sub>2</sub>, 1.25 NaH<sub>2</sub>PO<sub>4</sub>, 10 glucose; pH 7.4; 280-300 mOsm/L). The slices were kept in holding  
376 solution for at least 1.5 hours and gradually brought to room temperature.

377

378 *Chemicals used for electrophysiology*

379 The chemicals for the intracellular and extracellular solutions, glycine and strychnine  
380 hemisulfate salt were purchased from Sigma-Aldrich (St. Louis, MO, USA). Tetrodotoxin  
381 (TTX), 6-Imino-3-(4-methoxyphenyl)-1(6*H*)-pyridazinebutanoic acid hydrobromide  
382 (Gabazine), and 4-Hydroxyquinoline-2-carboxylic acid sodium salt (kynurenic acid sodium  
383 salt, KYNA) were purchased from the Tocris Bioscience (Bristol, UK).

384

385 *Data acquisition and analysis*

386 The slices were transferred to a submersion type recording chamber containing aCSF at 32-33  
387 °C and were perfused with aCSF at a rate of approximately 3 mL/min. TRH neurons were  
388 identified by the red fluorescence of the tdTomato under short epifluorescent illumination using  
389 an FN1 Microscope (Nikon, Tokio, Japan) equipped with 40x water-immersion objective with  
390 additional zoom (up to 2x) and Zyla CCD camera (ANDOR). Afterwards, the selected cell was  
391 studied under infrared differential interference contrast illumination. The patch pipettes (6-7  
392 MΩ) were pulled from borosilicate capillaries (OD=1.5 mm thin wall, Garner Co, Maharashtra,  
393 India.) with a P-1000 horizontal puller (Sutter Instrument Co., Novato, CA, USA). The  
394 intracellular pipette solution used for current-clamp ( $I=0$ ) electrophysiological recordings  
395 contained (in mM) 110 K-gluconate, 4 NaCl, 20 HEPES, 0.1 EGTA, 10 phosphocreatine di(tris)  
396 salt, 2 ATP, 0.3 GTP (pH 7.25; 280-300 mOsm/L). For sIPSC recording, the intracellular  
397 solution had the following composition: (in mM) 130 CsCl, 8 NaCl, 0.1 CaCl<sub>2</sub>, 0.1 EGTA, 10  
398 HEPES, 4 Mg-ATP, 0.3 Na<sub>2</sub>-GTP, 5 Lidocaine N-ethyl bromide (pH 7.25; 280–300 mOsm/L).  
399 Recordings were performed with a Multiclamp 700B patch clamp amplifier, Digidata-1440A  
400 data acquisition system and pCLAMP 10.4 software (Molecular Devices). The headstage of the  
401 amplifier was fitted onto a Luigs&Neumann SM7 micromanipulator system. Whole-cell  
402 current-clamp recordings were filtered at 10 kHz using the built-in Bessel filter of the amplifier

403 and digitized at 10 kHz. Slow and fast capacitive components were automatically compensated  
404 for. The stability of the patch was checked by repetitively monitoring the access resistance  
405 during the experiment, and TRH neurons in which the series resistance changed >25% were  
406 excluded from the statistics. Liquid junction potential was 14.4 mV and not compensated.

407

#### 408 *Whole-cell patch clamp recording*

409 After establishing a stable, whole-cell patch-clamp recording, a control period was recorded for  
410 2-3 min that was followed by a drug treatment phase for 3-4 min. First, the effect of glycine  
411 (0.5 mM) was measured on the firing frequency of TRH neurons in the presence or absence of  
412 the glycine receptor inhibitor, strychnine (125  $\mu$ M), in current-clamp mode (IC). Then, the  
413 voltage-dependent sodium channel inhibitor, TTX (1.2 mM), was added to the aCSF to prevent  
414 the potential indirect effects of glycine treatment, and the effect of glycine was also examined  
415 in the presence or absence of strychnine. The washout of the drugs restored the spiking  
416 frequency or the membrane potential of TRH neurons in all cases.

417 For glycinergic sIPSC recordings, cells were voltage clamped using a whole-cell clamp  
418 configuration at a holding potential of -63 mV, the average resting membrane potential of the  
419 TRH neurons. A control value was recorded for 2-3 min in the presence of Gabazine (3  $\mu$ M)  
420 and KYNA (1 mM) to inhibit the effects of the GABAergic or glutamatergic inputs, followed  
421 by application of strychnine in the presence of Gabazine and KYNA for 3-4 min.

422

#### 423 *Statistical analysis of the data of electrophysiological recordings*

424 Changes of spiking frequency, membrane potential and sIPSC recording were analyzed with  
425 Clampfit module of the pCLAMP 10.4 software (Molecular Devices, San José, CA, USA) and  
426 OriginPro 2015. Statistical analysis was performed using one-way analysis of variance  
427 (ANOVA) followed by the Bonferroni *post hoc* test to determine differences among treatment

428 groups in the current-clamp experiments, and the paired t-test was carried out in the voltage-  
429 clamp experiment. The number of studied cells is described in the results of each experiment.  
430 All data are reported as mean  $\pm$  standard error of mean (SEM). The  $p$  value  $<0.05$  was  
431 considered significant in all cases.

432

433

434 **RESULTS**

435 *Colocalization of tdTomato-immunoreactivity and proTRH mRNA in the PVN of TRH-IRES-*  
436 *tdTomato mice*

437 Drying results in fading of tdTomato's fluorescence, therefore its detection was performed by  
438 immunofluorescence in TRH-IRES-tdTomato mice. The distribution of tdTomato  
439 immunofluorescence (Fig. 1A) was found to be identical with the known distribution of TRH  
440 in the hypothalamus. *In situ* hybridization combined with immunofluorescence demonstrated a  
441 complete overlap between tdTomato-immunofluorescence and the *in situ* hybridization signal  
442 detecting the proTRH mRNA in the PVN. This demonstrated the selectivity and specificity of  
443 tdTomato expression in the generated *TRH-IRES-tdTomato* mice (Fig. 1B, C).

444

445 *TRH neurons receive GLYT2-IR innervation in the PVN*

446 GlyT2-IR axons were observed in close proximity to TRH-IR neurons in all subdivisions of the  
447 PVN where TRH neurons are located. By double-labeling immunofluorescence, large GLYT2-  
448 IR varicosities were observed on the surface of TRH-IR neurons (Fig 2). Quantification of the  
449 interaction of the two systems showed that GlyT2-IR axon varicosities established contacts with  
450  $53\pm 2\%$  of TRH neurons. An average of  $1.9\pm 0.1$  GlyT2-IR contacts were found on the surface  
451 of the innervated TRH neurons. At the ultrastructural level, synaptic associations were observed  
452 between NiDAB-labeled, GlyT2-IR varicosities and TRH neurons labeled with silver  
453 intensified colloidal gold particles (Fig. 3). Both axo-somatic and axo-dendritic synapses were  
454 found between the two systems. All of the observed synaptic associations were of the symmetric  
455 type, indicating the inhibitory nature of these inputs.

456

457 *TRH neurons express glycine receptors in the PVN*

458 To understand whether glycine released from axon terminals can influence TRH neurons in the  
459 PVN, the glycine receptor content of TRH neurons was studied in TRH-IRES-tdTomato mice.  
460 Punctuate GLYR-immunoreactivity was observed in all TRH neurons in all subdivisions of the  
461 PVN (Fig. 4).

462

463 *The ventrolateral PAG and the raphe magnus are the sources of the glycinergic input of TRH*  
464 *neurons in the PVN*

465 As a first step, the retrograde tracer CTB was injected into the PVN of GlyT2::GFP mice to  
466 investigate the origins of the glycinergic input of the PVN. CTB injection sites localized well  
467 within the borders of the PVN (Fig. 5) were used for the colocalization of CTB-  
468 immunoreactivity and GFP, the latter labeling glycinergic neurons. Double-labeled PVN  
469 projecting glycinergic neurons were observed in only two regions of the brainstem: in the RMg  
470 and VLPAG (Fig. 5).

471 To determine whether the TRH neurons of the PVN receive glycinergic input from both of these  
472 brainstem nuclei, hChR2(H134R)-eYFP fusion protein was expressed specifically in the  
473 glycinergic neurons of the RMg or the VLPAG of TRH-IRES-tdTomato//GlyT2::Cre mice  
474 using AAV mediated gene transfer. The AAV injection site was centered within the RMg in 4  
475 mice and in the VLPAG in 6 mice (Fig 6A, J). Axons of glycinergic neurons of RMg origin  
476 innervated symmetrically both parts of the PVN. While these axons densely innervated all  
477 parvocellular subdivisions of the PVN (Fig. 6 B-D), the magnocellular division of the PVN  
478 received less dense innervation. Glycinergic axons of VLPAG origin innervated primarily the  
479 ipsilateral side of the PVN, but sparse glycinergic axons were also observed on the contralateral  
480 side. Higher magnification images (Fig. 6E-I, N-Q) demonstrated that glycinergic axons  
481 originating from both the RMg and VLPAG contacted TRH neurons in all parvocellular

482 subdivisions of the PVN, demonstrating that the glycinergic input of TRH neurons originate  
483 from both the RMg and the VLPAG.

484

485 *Glycine inhibits the firing of TRH neurons in the PVN*

486 To understand the role of glycine in the regulation of TRH neurons, the effects of this amino  
487 acid transmitter was studied on the membrane potential and firing of TRH neurons in the mid  
488 level of PVN of TRH-IRES-tdTomato mice, where the hypophysiotropic TRH neurons are  
489 enriched (13). Application of glycine markedly decreased the membrane potential ( $-14.23 \pm 2.55$   
490 mV;  $n=6$ ,  $P<0.001$ ; Fig. 7) and completely blocked the firing (control:  $3.15 \pm 0.52$  Hz vs. glycine:  
491  $0.08 \pm 0.08$  Hz,  $n=6$ ,  $P<0.001$ ; Fig. 7) of TRH neurons. Co-application of strychnine completely  
492 prevented the glycine-induced changes of the membrane potential ( $0.16 \pm 1.65$  mV,  $P=1$  vs.  
493 control and  $P<0.001$  vs. glycine,  $n=6$ ; Fig. 7) and the firing rate ( $0.38 \pm 0.54$  Hz,  $P=1$  vs. control  
494 and  $P<0.001$  vs. glycine,  $n=6$ ; Fig. 7) of TRH neurons.

495 To understand whether the inhibitory effect of glycine is exerted directly on the TRH neurons,  
496 the effect of glycine was also studied in the absence of neuronal inputs in TTX (1.2 mM) treated  
497 slides. Application of glycine caused an approximately 6 mV hyperpolarization of TRH neurons  
498 (control:  $-63.20 \pm 0.94$  mV vs. Gly:  $-69.84 \pm 0.65$  mV,  $n=5$ ,  $P=0.0011$ ; Fig. 7 D, E) even in the  
499 presence of TTX. Application of strychnine abolished this effect of glycine ( $-64.11 \pm 1.58$  mV,  
500  $n=5$ ; Fig. 7 D, E).

501

502 *TRH neurons receive spontaneous inputs from glycinergic terminals*

503 To demonstrate the involvement of the glycinergic inputs in the regulation of TRH neurons of  
504 the PVN, the spontaneous glycinergic currents of these cells were studied in TRH-IRES-  
505 tdTomato mice. Glycinergic sIPSCs were isolated by simultaneous inhibition of the  
506 glutamatergic and GABAergic inputs with a mixture of KYNA and Gabazine. Despite the

507 presence of these inhibitors, sIPSCs were observed in 62.5% of TRH neurons. The frequency  
508 of these sIPSCs was  $0.824 \pm 0.19$  Hz (Fig. 8). Strychnine markedly decreased the frequency of  
509 these sIPSCs ( $0.12 \pm 0.04$  Hz,  $n=5$ ,  $P=0.038$ ; Fig. 8) suggesting that glycinergic synaptic inputs  
510 inhibit a population of TRH neurons. In 37.5% of the studied TRH neurons ( $n=3$ ), the frequency  
511 of sIPSCs was only  $0.080 \pm 0.014$  Hz after inhibition of GABAergic and glutamatergic currents  
512 cells with vs. without glycinergic sIPSC:  $P=0.028$ ). Strychnine had no effect on the sIPSC  
513 frequency of these cells ( $0.080 \pm 0.045$  Hz;  $P=0.963$ ).

514



515 **Discussion**

516 An important function of the HPT axis is to maintain stable thyroid hormone levels in the  
517 circulation under normal conditions and thus, to provide a continuous supply of thyroid  
518 hormones for tissues (8). This function is primarily controlled by the negative feedback effect  
519 of thyroid hormones on hypophysiotropic TRH neurons and pituitary thyrotrophs (8). Under  
520 certain conditions, such as fasting, infection or cold exposure, however, the activity of the HPT  
521 axis is altered by neuronal inputs or by the activity of tanycytes (8). Peptidergic inputs  
522 originating from the arcuate nucleus are known to mediate the effects of fasting and leptin  
523 treatment on the hypophysiotropic TRH neurons (8), while adrenergic innervation stimulates  
524 the hypophysiotropic TRH neurons during cold exposure (20). Our laboratories described that  
525 the TRH neurons of the PVN also receive inputs from neurons utilizing classical  
526 neurotransmitters such as GABA and glutamate (21, 22). Since glycinergic axons are also  
527 present in the PVN (3), we investigated whether TRH neurons are also controlled by glycine to  
528 regulate the thyroid axis.

529 To facilitate these studies, we generated a novel *knock in* mouse model expressing tdTomato  
530 specifically in TRH-producing cells using the CRISPR/Cas9 technology. By combined  
531 immunocytochemistry and *in situ* hybridization, we showed that there is a complete overlap of  
532 tdTomato protein and the proTRH mRNA in the PVN of these mice, indicating that the TRH-  
533 IRES-tdTomato mouse line allows specific identification of the TRH neurons. This new mouse  
534 line also enabled us to study the electrophysiology of TRH neurons and identify the TRH  
535 neurons in morphological studies without the use of colchicine, an axonal transport inhibitor.

536 Our presented data demonstrate that glycinergic neurons innervate approximately half of the  
537 TRH neurons in the PVN, establishing symmetric type synapsis suggesting the inhibitory nature  
538 of these connections (23, 24). In addition, we show that the vast majority of TRH neurons  
539 express glycine receptors. In agreement with these morphological findings, exogenous glycine

540 inhibited all TRH neurons studied in the PVN. Namely, glycine treatment markedly  
541 hyperpolarized TRH neurons and almost completely abolished the firing of these cells.

542 While approximately half of the TRH neurons received glycinergic innervation, almost all TRH  
543 neurons in the PVN contained glycine receptors and responded to glycine treatment. This  
544 discrepancy raised the question whether the sensitivity of the immunocytochemical method was  
545 insufficient to detect all of the glycinergic input to TRH neurons, or whether the glycine  
546 receptors of these neurons have other roles in addition to the detection of synaptically-released  
547 glycine. To address this question, we studied the glycinergic sIPSCs of TRH neurons.

548 After inhibition of glutamatergic and GABAergic currents, sIPSCs were still observed in  
549 approximately 60% of TRH neurons in the PVN. Administration of strychnine almost  
550 completely blocked the sIPSCs, demonstrating that endogenous glycine released from neuronal  
551 terminals exerts an inhibitory effect on TRH neurons in the PVN. However, glycinergic sIPSCs  
552 were not observed in approximately 40% of TRH neurons in the PVN. These data indicate that  
553 extrasynaptic glycine receptors are also involved in the regulation of TRH neurons.

554 In addition to glycine, taurine is also a known ligand of glycine receptors (25). In the supraoptic  
555 nucleus (SON), Deleuze et al (25) showed that the neurons express glycine receptors, but do  
556 not receive functional glycinergic synapses. Furthermore, they observed that the glycine  
557 receptor expressing cells are contacted by taurine containing astrocytes (22, 25). Based on these  
558 observations, they suggested that the ligand of glycine receptor in the SON is taurine, released  
559 from astrocytes (25). Thus, it seems feasible that TRH neurons in the PVN may also be  
560 regulated by both glycine, released from neuronal inputs, and by taurine, secreted by astrocytes  
561 and will require further investigation.

562 Although, glycinergic neurons are present in most parts of the brainstem, the origin of the  
563 glycinergic input to TRH neurons in the PVN is restricted to two, brainstem nuclei, the VLPAG  
564 and RMg. The role of these nuclei in the regulation of the TRH neurons and the HPT axis is

565 currently unknown. Published data, however, indicate that some of the conditions known to  
566 inhibit the HPT axis, such as the administration of bacterial lipopolysaccharide (LPS), a model  
567 of infection or different stressors (8), induces neuronal activation in the VLPAG and RMg (10,  
568 25-30). Thus, further studies are needed to determine whether projections from glycinergic  
569 neurons in these two, brainstem regions to TRH neurons in the PVN have a role in the mediation  
570 of the stress and LPS-induced inhibition of the hypophysiotropic TRH neurons and the HPT  
571 axis.

572 Glycinergic inputs of TRH neurons found not only in the mid level of the PVN, where the  
573 hypophysiotropic TRH neurons are concentrated (13), but also in other regions of the PVN, like  
574 in the anterior parvocellular subdivision, where the TRH neurons have no hypophysiotropic  
575 function (13). Therefore, our data indicate that glycine regulates both hypophysiotropic and  
576 non-hypophysiotropic populations of the TRH neurons in the PVN. Currently very little  
577 information is available about the function of non-hypophysiotropic TRH neurons of the PVN.  
578 The TRH neurons residing in the anterior parvocellular subdivision of the PVN were, however,  
579 shown to project to energy homeostasis-related areas, like the arcuate and ventromedial nuclei  
580 {Wittmann, 2009 #22}, thus it is feasible that the glycinergic neurons regulate the energy  
581 homeostasis via the non-hypophysiotropic TRH neurons.

582 In summary, these data demonstrate that TRH neurons in the PVN receive a functional,  
583 glycinergic input from the VLPAG and the RMg that exert an inhibitory effect on the TRH  
584 neurons, indicating that the glycinergic system may have an important role in the central  
585 regulation of the HPT axis. However, as not all TRH neurons in the PVN are innervated by  
586 glycinergic inputs yet responsive to glycine *in vitro*, we hypothesize that glial release of glycine  
587 or taurine, or yet another glycine receptor agonist, may also influence TRH neurons *via* glial-  
588 neuronal interactions.

589

590 **Acknowledgments**

591 This work was supported by Grants from the Hungarian Science Foundation (OTKA K124767),  
592 the Hungarian National Brain Research Program (2017-1.2.1-NKP-2017-00002) and EU  
593 H2020 THYRAGE no. 666869. The authors are very grateful to Dr. Hanns Ulrich Zeilhofer  
594 (University of Zurich, Zurich, Switzerland) for the kind gift of GLYT2::GFP and GLYT2::Cre  
595 mice.

596

597 **Author Disclosure Statement:**

598 The authors declare no competing financial interests.

599

600 **References**

- 601 1. Hernandez MS, Troncone LR 2009 Glycine as a neurotransmitter in the forebrain: a short  
602 review. *Journal of neural transmission* (Vienna, Austria : 1996) **116**:1551-1560.
- 603 2. Zafra F, Gomeza J, Olivares L, Aragon C, Gimenez C 1995 Regional distribution and  
604 developmental variation of the glycine transporters GLYT1 and GLYT2 in the rat CNS. *The*  
605 *European journal of neuroscience* **7**:1342-1352.
- 606 3. Zeilhofer HU, Studler B, Arabadzisz D, Schweizer C, Ahmadi S, Layh B, Bosl MR, Fritschy JM  
607 2005 Glycinergic neurons expressing enhanced green fluorescent protein in bacterial artificial  
608 chromosome transgenic mice. *The Journal of comparative neurology* **482**:123-141.
- 609 4. Poyatos I, Ponce J, Aragon C, Gimenez C, Zafra F 1997 The glycine transporter GLYT2 is a  
610 reliable marker for glycine-immunoreactive neurons. *Brain research Molecular brain research*  
611 **49**:63-70.
- 612 5. Zafra F, Gimenez C 2008 Glycine transporters and synaptic function. *IUBMB life* **60**:810-817.
- 613 6. Dutertre S, Becker CM, Betz H 2012 Inhibitory glycine receptors: an update. *The Journal of*  
614 *biological chemistry* **287**:40216-40223.
- 615 7. Johnson JW, Ascher P 1987 Glycine potentiates the NMDA response in cultured mouse brain  
616 neurons. *Nature* **325**:529-531.
- 617 8. Fekete C, Lechan RM 2014 Central regulation of hypothalamic-pituitary-thyroid axis under  
618 physiological and pathophysiological conditions. *Endocrine reviews* **35**:159-194.
- 619 9. Vavra V, Farkas E, Capraru O, Watanabe M, Fekete C, Bains JS 2014 Evidence for functional  
620 glycinergic transmission in the paraventricular nucleus of the hypothalamus Annual Meeting  
621 of the Society for Neuroscience, Washington, 124.101.
- 622 10. Foster E, Wildner H, Tudeau L, Haueter S, Ralvenius WT, Jegen M, Johannssen H, Hosli L,  
623 Haenraets K, Ghanem A, Conzelmann KK, Bosl M, Zeilhofer HU 2015 Targeted ablation,  
624 silencing, and activation establish glycinergic dorsal horn neurons as key components of a  
625 spinal gate for pain and itch. *Neuron* **85**:1289-1304.
- 626 11. Singh P, Schimenti JC, Bolcun-Filas E 2015 A mouse geneticist's practical guide to CRISPR  
627 applications. *Genetics* **199**:1-15.
- 628 12. Albagli-Curiel O, Lecluse Y, Pognonec P, Boulukos KE, Martin P 2007 A new generation of  
629 pPRIG-based retroviral vectors. *BMC biotechnology* **7**:85.
- 630 13. Kadar A, Sanchez E, Wittmann G, Singru PS, Fuzesi T, Marsili A, Larsen PR, Liposits Z, Lechan  
631 RM, Fekete C 2010 Distribution of hypophysiotropic thyrotropin-releasing hormone (TRH)-  
632 synthesizing neurons in the hypothalamic paraventricular nucleus of the mouse. *The Journal*  
633 *of comparative neurology* **518**:3948-3961.
- 634 14. Fekete C, Mihaly E, Luo LG, Kelly J, Clausen JT, Mao Q, Rand WM, Moss LG, Kuhar M, Emerson  
635 CH, Jackson IM, Lechan RM 2000 Association of cocaine- and amphetamine-regulated  
636 transcript-immunoreactive elements with thyrotropin-releasing hormone-synthesizing  
637 neurons in the hypothalamic paraventricular nucleus and its role in the regulation of the  
638 hypothalamic-pituitary-thyroid axis during fasting. *The Journal of neuroscience : the official*  
639 *journal of the Society for Neuroscience* **20**:9224-9234.
- 640 15. Wittmann G, Fuzesi T, Liposits Z, Lechan RM, Fekete C 2009 Distribution and axonal projections  
641 of neurons coexpressing thyrotropin-releasing hormone and urocortin 3 in the rat brain. *J*  
642 *Comp Neurol* **517**:825-840.
- 643 16. Hondo M, Furutani N, Yamasaki M, Watanabe M, Sakurai T 2011 Orexin neurons receive  
644 glycinergic innervations. *PloS one* **6**:e25076.
- 645 17. Wittmann G, Fuzesi T, Liposits Z, Lechan RM, Fekete C 2009 Distribution and axonal projections  
646 of neurons coexpressing thyrotropin-releasing hormone and urocortin 3 in the rat brain. *The*  
647 *Journal of comparative neurology* **517**:825-840.
- 648 18. Branchereau P, Van Bockstaele EJ, Chan J, Pickel VM 1995 Ultrastructural characterization of  
649 neurons recorded intracellularly in vivo and injected with lucifer yellow: advantages of  
650 immunogold-silver vs. immunoperoxidase labeling. *Microscopy research and technique*  
651 **30**:427-436.

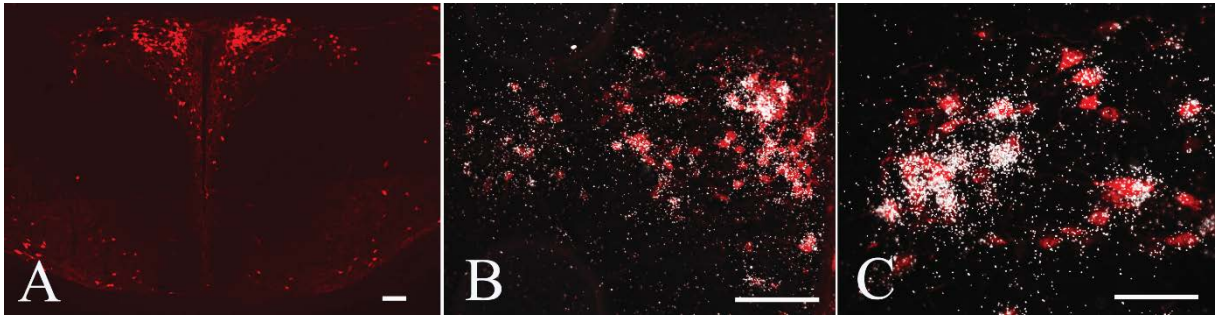
- 652 19. Paxinos G, Watson C 1998 The Rat Brain in Stereotaxic Coordinates. Academic Press, San Diego,  
653 CA.
- 654 20. Wittmann G 2008 Regulation of hypophysiotrophic corticotrophin-releasing hormone- and  
655 thyrotrophin-releasing hormone-synthesising neurones by brainstem catecholaminergic  
656 neurones. *Journal of neuroendocrinology* **20**:952-960.
- 657 21. Fekete C, Wittmann G, Liposits Z, Lechan RM 2002 GABA-ergic innervation of thyrotropin-  
658 releasing hormone-synthesizing neurons in the hypothalamic paraventricular nucleus of the  
659 rat. *Brain research* **957**:251-258.
- 660 22. Wittmann G, Lechan RM, Liposits Z, Fekete C 2005 Glutamatergic innervation of corticotropin-  
661 releasing hormone- and thyrotropin-releasing hormone-synthesizing neurons in the  
662 hypothalamic paraventricular nucleus of the rat. *Brain research* **1039**:53-62.
- 663 23. Peters A, Palay SL, deF Webster H 1991 The fine structure of the nervous system. Neurons and  
664 their supporting cells. Third Edition ed. Oxford University Press, Oxford.
- 665 24. Somogyi P, Soltesz I 1986 Immunogold demonstration of GABA in synaptic terminals of  
666 intracellularly recorded, horseradish peroxidase-filled basket cells and clutch cells in the cat's  
667 visual cortex. *Neuroscience* **19**:1051-1065.
- 668 25. Deleuze C, Alonso G, Lefevre IA, Duvoid-Guillou A, Hussy N 2005 Extrasynaptic localization of  
669 glycine receptors in the rat supraoptic nucleus: further evidence for their involvement in glia-  
670 to-neuron communication. *Neuroscience* **133**:175-183.
- 671 26. Furlong TM, McDowall LM, Horiuchi J, Polson JW, Dampney RA 2014 The effect of air puff  
672 stress on c-Fos expression in rat hypothalamus and brainstem: central circuitry mediating  
673 sympathoexcitation and baroreflex resetting. *The European journal of neuroscience* **39**:1429-  
674 1438.
- 675 27. Devall AJ, Lovick TA 2010 Differential activation of the periaqueductal gray by mild anxiogenic  
676 stress at different stages of the estrous cycle in female rats. *Neuropsychopharmacology* :  
677 official publication of the American College of Neuropsychopharmacology **35**:1174-1185.
- 678 28. Lino-de-Oliveira C, de Oliveira RM, Padua Carobrez A, de Lima TC, del Bel EA, Guimaraes FS  
679 2006 Antidepressant treatment reduces Fos-like immunoreactivity induced by swim stress in  
680 different columns of the periaqueductal gray matter. *Brain research bulletin* **70**:414-421.
- 681 29. Lino-de-Oliveira C, Sales AJ, Del Bel EA, Silveira MC, Guimaraes FS 2001 Effects of acute and  
682 chronic fluoxetine treatments on restraint stress-induced Fos expression. *Brain research*  
683 *bulletin* **55**:747-754.
- 684 30. Imbe H, Murakami S, Okamoto K, Iwai-Liao Y, Senba E 2004 The effects of acute and chronic  
685 restraint stress on activation of ERK in the rostral ventromedial medulla and locus coeruleus.  
686 *Pain* **112**:361-371.

687

688

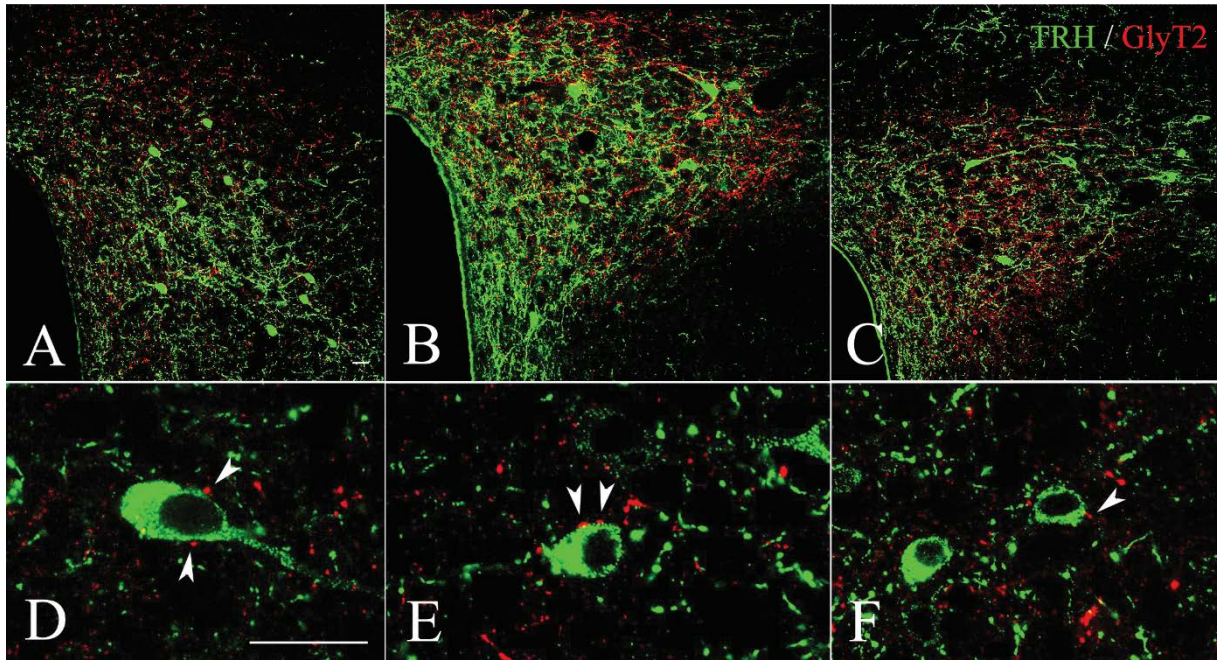
689

690 **Figures**



692 **Figure 1.** Characterization of the TRH-IRES-tdTomato mice. Low magnification image (A)  
693 illustrates that the distribution of the tdTomato-immunoreactivity in the TRH-IRES-tsTomato  
694 mice is identical with the known distribution of TRH in the hypothalamus. Double-labeling  
695 combined in situ hybridization and immunofluorescence (B) demonstrate the complete overlap  
696 of tdTomato (red) and proTRH mRNA (silver grain) in the PVN. Higher magnification image  
697 (C) shows the colocalization of the two signals in the PVN. Scale bars on A and B = 100 $\mu$ m,  
698 on C = 50 $\mu$ m.

699



700

701 **Figure 2.** Relationship of GLYT2-IR axons and TRH-IR neurons in the PVN of CD1 mice.

702 GlyT2-IR (red) axons were observed in close proximity of the TRH-IR (green) neurons in all

703 subdivisions of the PVN. A-C figures show the relationship of GLYT2-IR axons and TRH

704 neurons in the anterior (A), mid (B) and posterior (C) levels of the PVN. Higher magnification

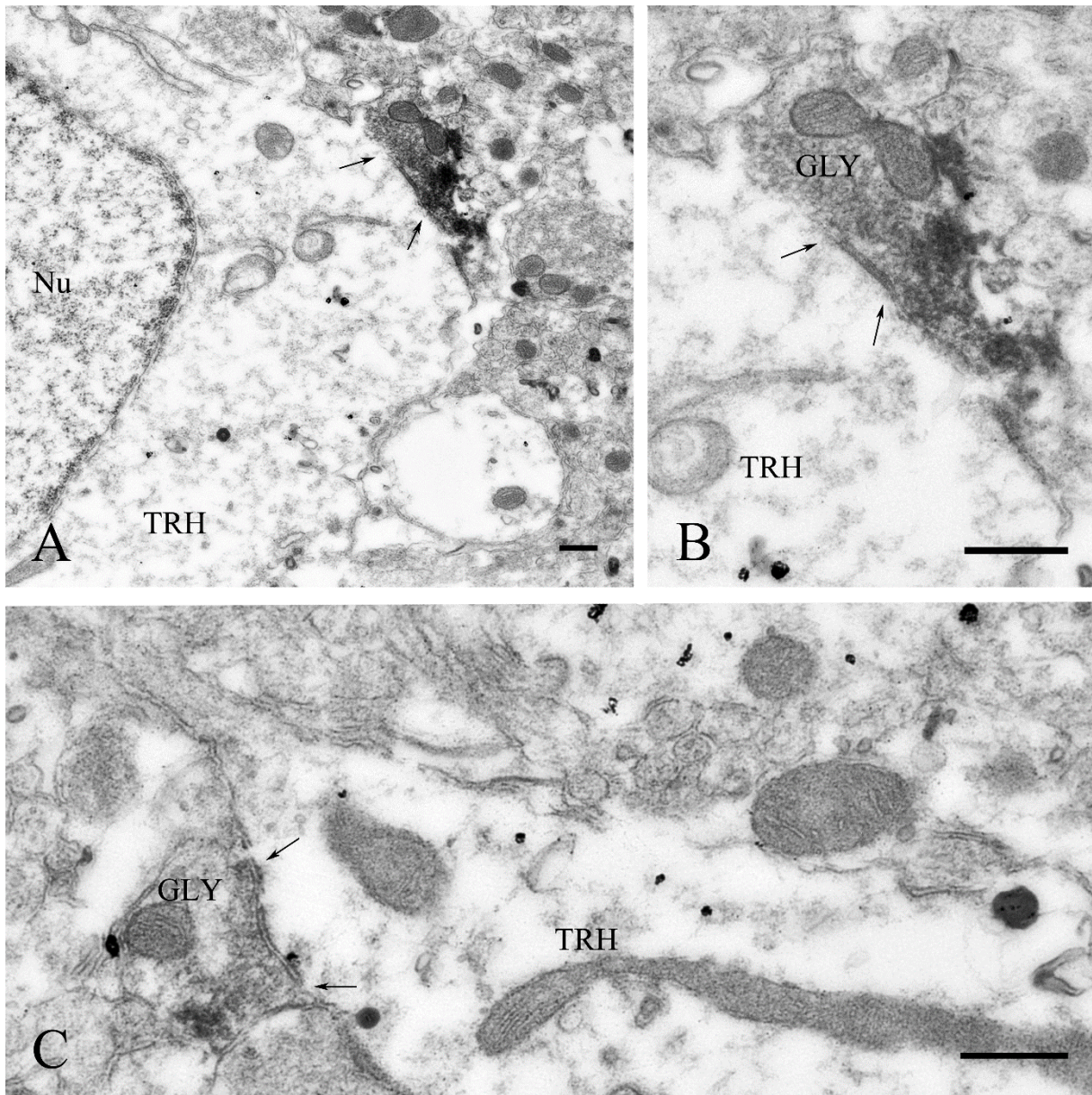
705 images illustrate the GLYT2-IR boutons (arrowheads) on the surface of TRH neurons in the

706 anterior (D), mid (E) and posterior (F) levels of the PVN. Scale bars= 20  $\mu$ m, Scale bar on A

707 corresponds to A-C, Scale bar on D corresponds to D-F.

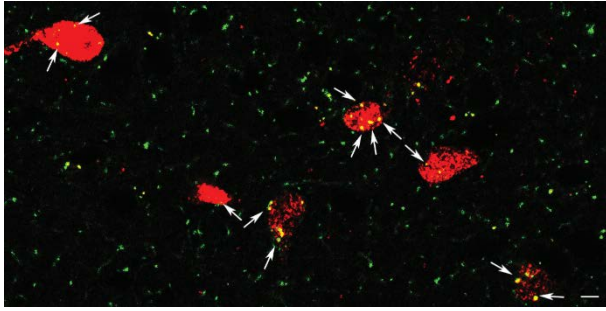
708





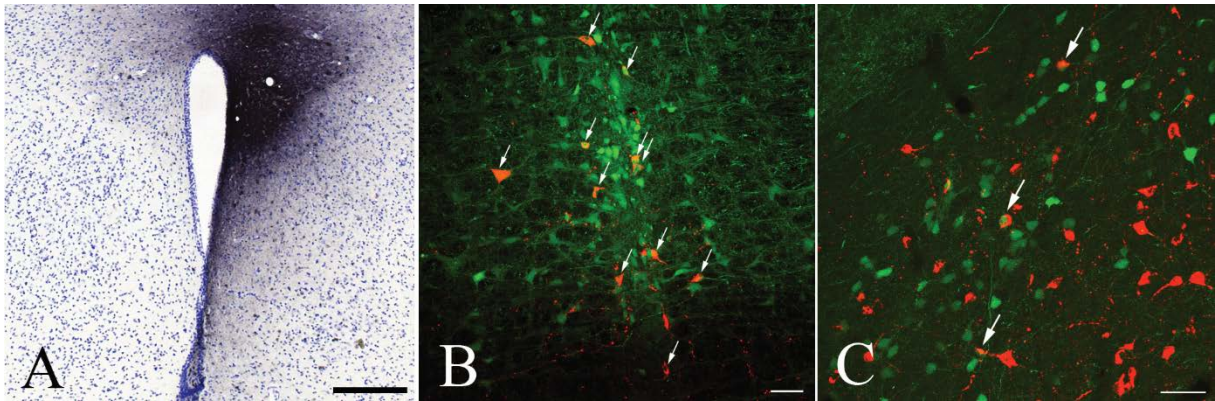
709

710 **Figure 3.** GLYT2-IR varicosities establish symmetric type synapses on TRH neurons in the  
 711 PVN of CD1 mice. At the ultrastructural level, synaptic associations were observed between  
 712 NiDAB labeled GlyT2-IR varicosities and TRH neurons labeled with silver intensified colloidal  
 713 gold particles. Both axo-somatic (A, and in higher magnification on B), and axo-dendritic  
 714 synapses (C) were found between the two systems. These synaptic associations were of  
 715 symmetric type indicating the inhibitory nature of these inputs. Scale bar: 200 nm.



716

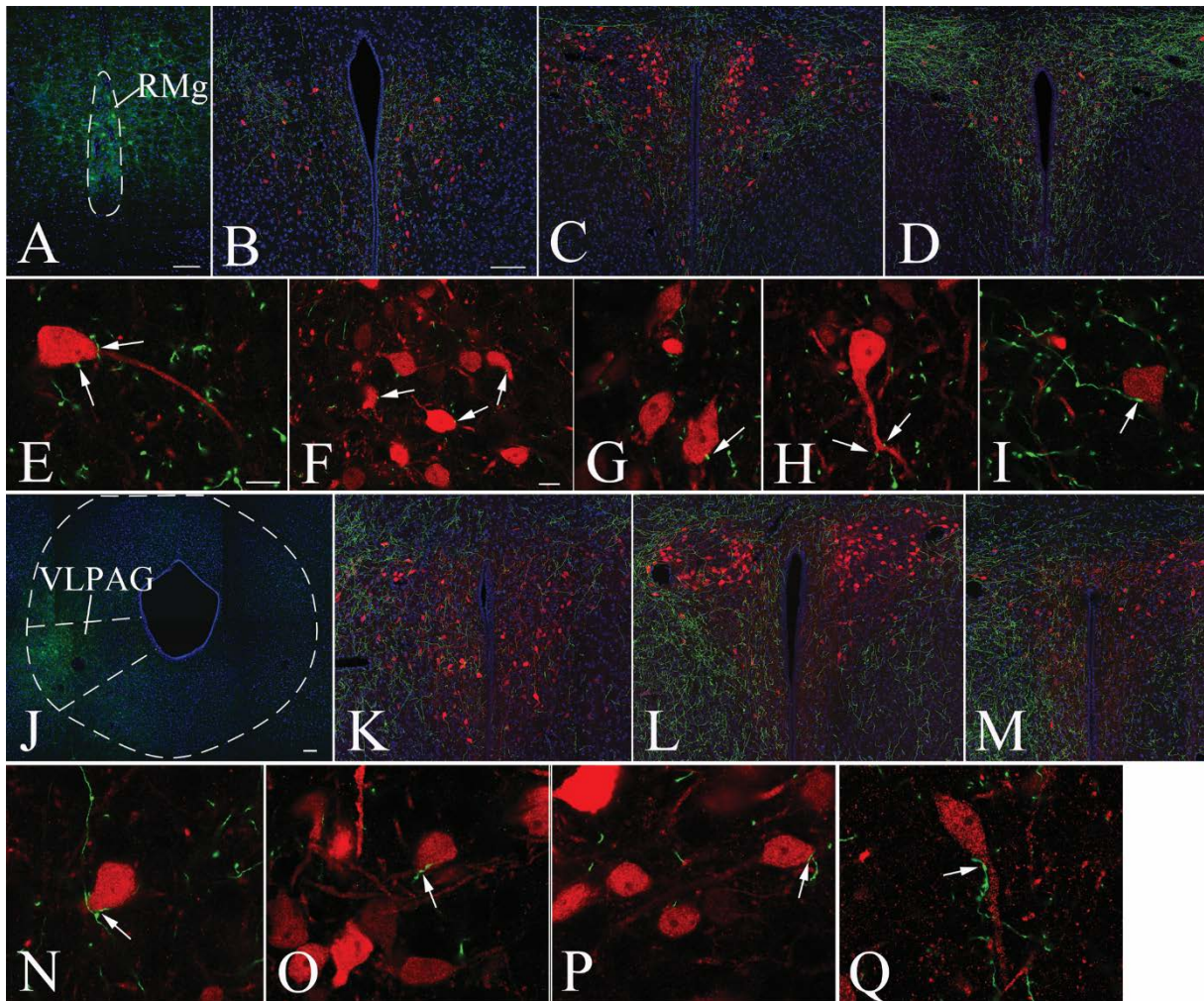
717 **Figure 4.** Presence of glycine receptor-immunoreactivity in the TRH neurons in the PVN of  
 718 TRH-IRES-tdTomato mice. Punctuate glycine receptor-immunoreactivity (green) is present in  
 719 all TRH neurons (red) studied. Scale bar = 5 $\mu$ m



720

721 **Figure 5.** Origin of the glycinergic input of the PVN of GLYT2::GFP mice. (A) illustrates a  
 722 representative CTB injection site. The CTB immunoreactivity was visualized using NiDAB  
 723 chromogen. Nissl staining was used to facilitate the identification of the borders of the PVN.  
 724 Immunofluorescent preparations demonstrate the presence of the PVN projecting (red, CTB-  
 725 immunoreactive) glycinergic neurons (green, GLYT2-GFP) in the RMg (B) and VLPAG (C).  
 726 Arrows point to the double-labeled neurons. Scale bar on A = 200 $\mu$ m, on B and C = 50 $\mu$ m.





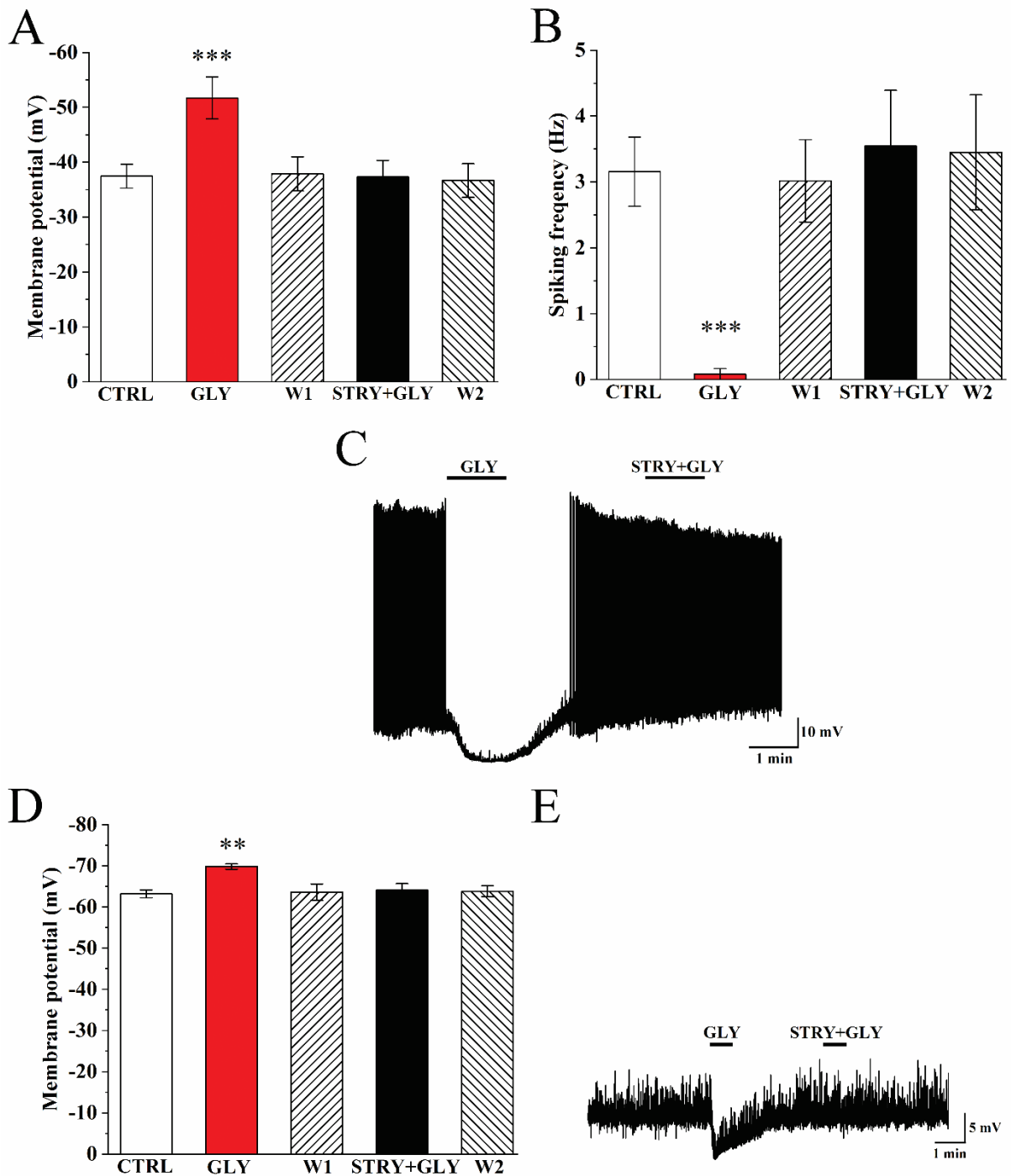
727

728 **Figure 6.** Involvement of the glycinergic neurons of the RMg and VLPAG in the innervation  
 729 of the TRH neurons in the PVN of TRH-IRES-tdTomato//GlyT2::Cre mice. A representative  
 730 image (A) illustrates the AAV mediated expression of hChr2(H134R)-eYFP fusion protein  
 731 (green) in RMg glycinergic neurons of TRH-IRES-tdTOMATO//GlyT2-Cre mice. Low  
 732 magnification images illustrate the distribution of the glycinergic axons (green) in the  
 733 parvocellular subdivisions of the PVN of originating from the RMg and their relationship to the  
 734 TRH neurons (red) in the anterior (B), mid (C) and (D) posterior levels of the PVN. While the  
 735 glycinergic axons originating from the RMg densely innervate the parvocellular subdivisions  
 736 on both sides of the hypothalamus, only low density of axons are observed in the magnocellular  
 737 subdivision (C). High magnification images demonstrate the juxtaposition of glycinergic axons

738 of RMg origin to TRH neurons in the anterior (E), mid (F-H) and posterior (I) levels of the  
739 PVN.

740 A representative image (J) illustrates the AAV-mediated expression of hChR2(H134R)-eYFP  
741 fusion protein in glycinergic neurons of VLPAG of TRH-IRES-tdTOMATO//GlyT2-Cre mice.

742 Low magnification images illustrate the distribution of the glycinergic axons of VLPAG origin  
743 in the parvocellular subdivision of the PVN and their relationship to TRH neurons (red) at the  
744 anterior (K), mid (L) and (M) posterior levels of the PVN. The glycinergic input of VLPAG  
745 origin primarily innervates the ipsilateral side, but axons can also be observed on the  
746 contralateral side. High magnification images demonstrate the juxtaposition of the glycinergic  
747 axons of VLPAG origin to TRH neurons at the anterior (N), mid (O,P) and posterior (Q) levels  
748 of the PVN. DAPI counterstaining (blue) was used to facilitate the identification of brain  
749 regions (A-D, J-M). Arrows point to glycinergic axons juxtaposed to TRH neurons. Scale bar  
750 on A and J = 100  $\mu\text{m}$ ; on B = 100  $\mu\text{m}$  corresponds to B-D and K-L; on E = 10  $\mu\text{m}$  corresponds  
751 to E, G-I and N-Q; on F = 10  $\mu\text{m}$ .



752

753 **Figure 7.** Effect of glycine on the membrane potential and the spiking frequency of TRH

754 neurons. Bar graphs show changes of membrane potential (A) and the firing frequency (B) of

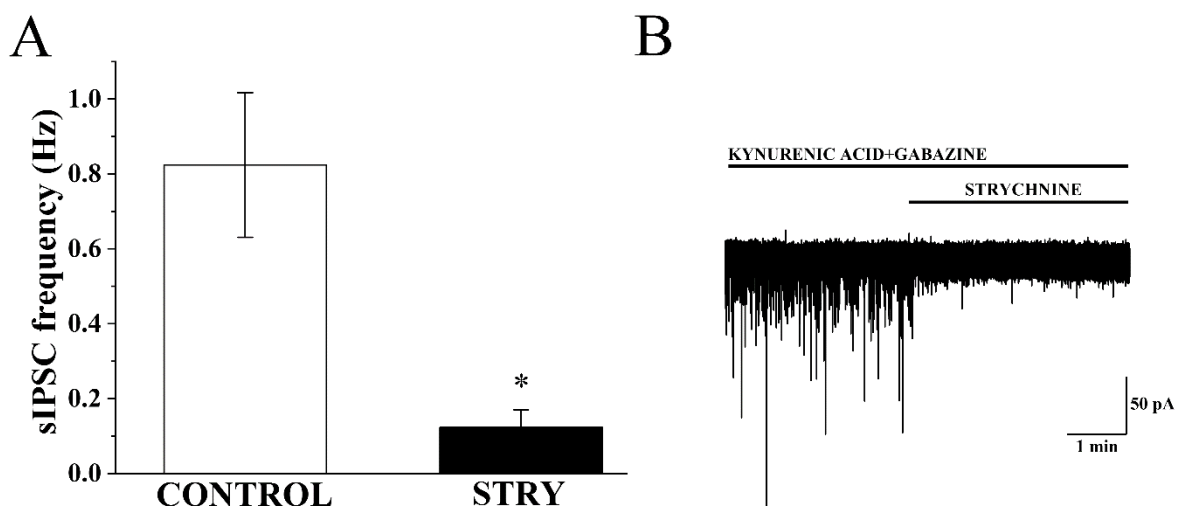
755 TRH neurons in a response to glycine in the presence or absence of the glycine receptor

756 inhibitor, strychnine. Glycine, alone, decreased the membrane potential and completely

757 inhibited the firing of TRH neurons. Strychnine prevented these effects of glycine.

758 Representative trace (C) illustrates the effects of glycine on the membrane potential and firing

759 rate of a TRH neuron, and the absence of the glycine-induced changes when strychnine is co-  
760 administered. To understand whether this effect of glycine is exerted directly on the TRH  
761 neurons, the effect of glycine was studied in the presence of TTX. Bar graph (D) shows the  
762 change of the membrane potential of TRH neurons in the presence of TTX in a response to  
763 glycine in the presence or absence of the glycine receptor inhibitor, strychnine. A representative  
764 trace is shown on (E). Bath application of glycine depolarized the TRH neurons in the presence  
765 of TTX. Strychnine completely prevented this effect of glycine. \*\* or \*\*\* labels significant  
766 difference ( $P < 0.01$  or  $P < 0.001$ , respectively) based on repeated measure ANOVA followed by  
767 Bonferroni *post hoc* test. Data are expressed as mean  $\pm$  SEM. Abbreviations: control – CTRL,  
768 glycine – GLY, washout – W and strychnine – STRY.



769  
770 **Figure 8.** Examination of glycinergic spontaneous inhibitory postsynaptic currents on TRH  
771 neurons. Bar graph (A) shows the average frequency of the sIPSCs of TRH neurons in the  
772 presence of glutamate and GABA receptor inhibitors and the effect of strychnine on the  
773 frequency of these currents. A representative trace illustrates that application of strychnine  
774 markedly inhibited the sIPSCs of TRH neurons in the presence of KYNA and gabazine.  
775 \* presents significant difference ( $P < 0.05$ ) based on the paired sample t-test. Data are expressed  
776 as mean  $\pm$  SEM. Abbreviations: strychnine – STRY.